SERVICE AND ULTIMATE BEHAVIOUR OF SLIM FLOOR BEAMS: AN EXPERIMENTAL STUDY

Nadia Baldassino[1], Giacomo Roverso[1], Gianluca Ranzi[2], Riccardo Zandonini[1]

[1]*Department of Civil, Environmental and Mechanical Engineering, University of Trento, Trento, Italy*

[2] *School of Civil Engineering, The University of Sydney, Sydney, Australia*

Slim floor systems represent an economical and competitive solution for building applications that combine the advantages of concrete floors, prefabricated steel sections and a shallow depth. The distinctive feature of this form of construction relies on the fact that the lower steel flange is wider than the top flange to provide a continuous support along the beam length for the slab formwork. The latter is usually specified in the form of either profiled sheeting or cellular slabs. In this structural typology, the steel section is embedded within the thickness of the slab.

This paper presents an experimental study aimed at evaluating the service behaviour of slim floor beams induced by the time-dependent behaviour of the concrete and at establishing the possible influence of creep effects on their ultimate response. For this purpose, two slim floor samples were prepared in a simply-supported configuration. Their long-term deflections and deformations were monitored over time for about ten months, after which the specimens were tested to failure. The specimens possessed identical concrete and steel geometries. The shear connection was provided by transverse steel reinforcing bars installed within regularly spaced holes incorporated in the steel web. The samples were cast unpropped so that the self-weight of the wet concrete was carried by the steel member. The only difference between the two specimens consisted in the loading history specified over time. In particular, one slim floor sample was kept unloaded for the entire duration of the test to monitor the influence of shrinkage effects while the second specimen was subjected to a sustained load to evaluate the effects of both creep and shrinkage. The experimental data reported in this study provides insight into their long-term and ultimate response, and valuable benchmarking data for the calibration of numerical models and design procedures related to the serviceability and ultimate limit states of slim floor systems.

Keywords: composite, concrete time effects, service behaviour, slim floor.

1. INTRODUCTION

Composite steel-concrete beams and slabs are widely used throughout the world for building applications. Among composite solutions, slim floor beams have been popular and adopted in steel framed structures, particularly in Europe [1-3]. With this structural typology, the steel section is embedded within the thickness of the slab and the lower flange of the steel joist is specified wider than the top flange to provide a continuous support along the beam length for the floor formwork that could consist of either profiled sheeting or cellular slabs. The use of slim floors can lead to shallow floor thicknesses and can enhance construction speed. Applications in Europe have shown that the use of slim floor beams is commercially competitive for spans in the range between 5 m and 9 m. For example, this form of construction has been adopted in Scandinavian countries in combination with prefabricated hollow core slabs, while in other European countries this solution has been usually applied with in-situ concrete pours. Over the last decades, proprietary steel beam solutions have been developed and are available on the market to support this floor typology. Initial work on slim floor solutions was carried out in the 90's, e.g. [4-11], and this supported the wide-spread use of this form of construction. Over the last decades, the number of studies investigating slim floor systems has been increasing, with particular focus devoted at the development of shear connection typologies for efficient construction, for example, by varying the profile of the beam, the web opening for possible dowel actions and the reinforcement arrangement, e.g. [2, 11-23]. As occurred for other composite floor typologies [24], most of the research carried to date on slim floors has focused at its ultimate response and, despite the wide adoption of this solution, there are no specific European guidelines for this type of building floor [25]. To the knowledge of the authors, no experimental work has been carried out to investigate the time-dependent response of slim floor beams. This limited attention devoted to time effects is not specific to slim floor systems but is representative of a historical trend observed for research carried out over the years on composite structure that mainly focussed on its ultimate response to characterise the shear connection behaviour

and how this could influence the member resistance, e.g. [24]. The limited research that focused on service performance of slim floor beams aimed at the characterisation of the effective width and at the calculation of the flexural rigidities to be used for deflection limit state, e.g. [26]. In this case, the proposed procedure was validated against test results performed on simply-supported samples subjected to short-term loading.

In this context, this paper intends to provide new experimental data related for the long-term and ultimate behaviour of slim floor beams in which the shear connection is provided by the installation of transverse reinforcing bars through holes placed in the steel web. In this study, two companion slim floor samples were prepared with identical concrete and steel geometries. The samples were cast unpropped and they varied for the specified loading history, i.e. one specimen was maintained unloaded to monitor the time-dependent influence of shrinkage and one sample was subjected to a sustained load to evaluate its creep and shrinkage effects. At the completion of the long-term study, the specimens were tested to failure to evaluate the possible influence of creep produced by the sustained load on the ultimate response. Despite the reported experimental programme includes only two samples, these provide useful data for the calibration and benchmarking of numerical and design models.

2. PREPARATION OF SPECIMENS

The experimental work presented in this paper describes the long-term and ultimate tests performed on two slim floor beam samples, referred to as SF1 and SF2 in the following. The composite cross-section was composed by a HEB200 steel beam (doubly-symmetric steel section with 200 mm × 15 mm flange and 170 mm × 9 mm web, and 400 mm × 15 mm plate welded to underside of steel flange) and a concrete T-shaped slab whose flange had a width of 2000 mm and thickness of 120 mm while its web was 300 mm wide, as illustrated in Figure 1.

The beams were prepared and tested in a simply-supported configuration. The total length of the members was 6300 mm and the internal span in between roller supports was 6000 mm. The specimens were cast

under unpropped conditions. This was achieved by supporting the formwork on longitudinal timber joists that were carried by transverse timber members bolted to the underside of the steel section as shown in Figure 2. For this purpose, steel bolts were welded to the steel bottom flange at a spacing of about 1000 mm as depicted in Figures 2a and 2b. With this approach, the self-weight of the beam (i.e. steel joist and wet concrete) was carried by the steel section during casting. Once the concrete hardened, it was assumed to be unloaded and, therefore, subjected to only shrinkage effects [27].

The steel reinforcement consisted of a square welded mesh (with 8 mm diameter steel bars welded at 200 mm spacings in both directions) placed over the top of the steel beam as shown in Figure 1b. Transverse steel reinforcing bars of 16 mm diameter were installed at 500 mm spacings through the 40 mm diameter holes prepared in the steel web to contribute to the shear connection between the concrete and steel components (Figure 1b). A curing compound was applied to the concrete slab after the pour following typical industry practice.

3. LONG-TERM EXPERIMENTS

3.1 Overview

Specimens SF1 and SF2 were monitored for a period of about 10 months. In particular, the formwork was removed after a month and the monitoring started soon afterwards. Sample SF1 was maintained unloaded (i.e. no external load applied to the beam) for the entire duration of the long-term test, while specimen SF2 was subjected, after 3 months from casting, to an applied service load of 300 kN (distributed along the member length). In this manner, specimen SF2 was subjected to both creep (produced by the sustained load) and the time-dependent effects induced by shrinkage, while the response of sample SF1 was assumed to be influenced by the time-dependent behaviour associated to shrinkage effects only. In order to gain insight into the shrinkage response that has been shown in the literature to significantly affect the composite service response [28-30], the loading of sample SF2 was delayed to provide a three month period over which to compare the long-term measurements of specimens SF1 and

SF2. A high level of sustained load was selected to gain insight into the long-term response of the shear connection when approaching the beginning of its nonlinear behaviour measured from push-out tests, e.g. [31].

3.2 Layout of instrumentation

The beam samples were instrumented with LVDTs and strain gauges to capture the time-dependent displacements and deformations. In the case of specimen SF2, 5 LVDTs were used to monitor the deflections, i.e. 3 sensors were placed at mid-span (referred to as TR-1, TR-2 and TR-3) and 2 at the quarter points (denoted as TR-4 and TR-5) as depicted in Figures 3a and 3b. For sample SF1, only the mid-span deflection (TR-1) was monitored over time.

The end slips were measured in both specimens at the heights of the steel flanges as shown in Figures 3a and 3c, and the corresponding LVDTs were referred to as TR-6, TR-7, TR-8 and TR-9.

Deformations were monitored on both samples at 9 locations at mid-span as specified in Figure 3b. In particular, 4 strain gauges were used to capture the deformations induced in the steel section (referred to as SG-1, SG-2, SG-3 and SG-4) and the remaining 5 strain gauges were applied to the top and bottom of the concrete slab (denoted as SG-1bis, SG-5, SG-6, SG-7 and SG-8), as described in Figure 3b.

3.3 Application of sustained load on sample SF2

Specimen SF2 was loaded at 99 days from casting with an external uniformly distributed load. This was achieved by placing metal cages filled with rocks on transverse spreader beams distributed along the member span. Different stages of the load application are shown in Figure 4. The external load was kept on the sample for a period of about 9 months.

3.4 Long-term response

The long-term monitoring of specimens SF1 and SF2 started 41 days from concrete casting, i.e. on 15 May 2017. As a reference for the graphs provided, the casting of the specimens took place on 4 April

2017. The long-term datalogging terminated after about 11 months from concrete casting for sample SF1 (i.e. on 7 March 2018) and after one year for specimen SF2 (i.e. on 4 April 2018). All long-term data reported in this paper has been plotted against these dates.

The variations of the deflections over time are plotted in Figure 5. In the case of sample SF1, a slight increase in mid-span deflections was observed during the first 3-4 months from casting due to shrinkage, as depicted in Figure 5a. At this point in time, a transversal crack developed through the thickness of the sample that released part of the stresses induced by shrinkage and produced a sudden reduction in the mid-span deflection, after which no significant variations in deflections were noted till the end of the long-term test. In the case of specimen SF2, similar deflections to those measured for sample SF1 were recorded before the application of the sustained load (i.e. applied between 12 and 13 July 2017). The fact that both samples responded in a similar fashion was a useful experimental verification for the adequacy of the long-term measurements, especially in the case of time-dependent tests that are governed by smaller deformations and deflections than experiments carried out to failure. In the broader context of research carried out for the service response of slim floor systems, the reported measurements are expected to provide a useful reference for the benchmarking of the long-term response against other long-term tests and for the calibration of numerical and design models. After the application of the external load, the deflections were then subjected to both creep and shrinkage effects (Figure 5b). A transverse crack occurred also in the case of specimen SF2 after 3-4 months when the beam was already subjected to the external sustained load. In this case, the crack was only noted on one side of the slab (this was attributed to the fact that SF2 was subjected to the sustained load at this time).

The variations of the slip measurements remained very small for the duration of the long-term tests as shown in Figure 6. During the unloaded conditions (i.e. entire test for SF1 and first few months for SF2), shrinkage effects induced shortening in the concrete and, therefore, a relative movement at the member ends in which the concrete moved inwards (i.e. towards the mid-pan). Upon application of the sustained

load, the end slips observed for sample SF2 changed sign to resist the applied external load. At the end of the test, the average slips at the two member ends of sample SF1 were 0.5 mm and 0.35 mm, while those exhibited by specimen SF2 were below -0.2 mm (in the opposite direction of those measured for SF1 because of the presence of the external load).

The time-dependent variation of the strain gauge readings is presented in Figure 7. In the first 3-4 months there is a clear shortening of the slab induced by shrinkage, for example, well captured in specimen SF1 by the top concrete strain gauges, i.e. SG-1bis, SG-5 and SG-6 (Figure 7a). The transverse crack mentioned earlier through the slab cross-section occurred within the length of strain gauge SG-1bis and compromised the measurement of this sensor afterwards. The strains recorded at the bottom steel flange (i.e.SG-2, SG-3 and SG-4) remained small, i.e. within 30 με, while the top face of the slab continued to shorten for the entire duration of the test.

A similar trend was observed for sample SF2 in the first few months from testing. The application of the sustained load induced larger flexural deformations. By considering the strain readings recorded through the cross-section it was possible to determine the time-dependent variation of the location of the neutral axis from the time of loading, as depicted in Figure 8. The key observation from this figure relied on the fact that the shear connection, i.e. reinforcing bar through web hole, remained above the neutral axis till the end of the test and, therefore, the shear connection was located in the compressed part of the section (even if the compression in the web hole area was relatively small due to its vicinity to the neutral axis).

The variations of the ambient temperature and relative humidity recorded in the vicinity of the samples during the long-term tests is reported in Figure 9. The average values measured during this period were 21.3° C and 49.6% for the temperature and relative humidity, respectively.

4. ULTIMATE EXPERIMENTS

4.1 Overview

At the completion of the long-term tests, samples SF1 and SF2 were tested to failure as described below.

4.2 Loading arrangement and layout of instrumentation

The beam samples were tested in a simply-supported configuration and the load was applied by means of two central line loads placed perpendicular to the member axis and located at 750 mm on each side from the mid-span (Figure 10).

The instrumentation layout installed on both samples was similar to the one adopted for the long-term test of specimen SF2 with the addition of four LVDTs at the member quarter points to monitor the deflection over the slab flanges (denoted as TR-6, TR-7, TR-8 and TR-9) and of two strain gauges on the top surface of the slab at mid-span near the slab edges to monitor the possible occurrence of shear-lag effects at different levels of load (Figure 3).

4.3 Ultimate response

Samples SF1 and SF2 exhibited a similar response during the ultimate tests as shown in Figure 11. The load cycles included in the testing protocol were required to reset the actuator when it reached the end of its stroke. After unloading, packing was placed below the actuator and the specimen was reloaded. This process was repeated two times for sample SF1 and once for specimen SF2. The peak loads resisted by specimens SF1 and SF2 were 536.4 kN and 562.7 kN, respectively (Figure 11). In this case, creep effects did not appear to have influenced the composite carrying capacity because the measured peak loads were within 5% variation from each other and the sample subjected to a sustained load exhibited a greater resistance. The corresponding material properties measured for the concrete and steel components at the time of the ultimate tests were: average concrete compressive cylinder strength of 43.6 MPa, yield and ultimate strengths of the steel section (HEB200) were 438 MPa and 510 MPa, respectively, and yield and ultimate strengths of the steel plate welded on the underside of the HEB200 section were 455 MPa and 525 MPa, respectively.

Both samples exhibited good ductility and the tests were terminated once the load-displacement curves started its softening part at a mid-span deflection of about 380 mm. The failure mode exhibited in both cases consisted of concrete crushing.

In the initial loading phase, sample SF1 exhibited a response that could be regarded as linear until the load of 383 kN was reached as highlighted in Figure 11a. At this point, the slip at one end of the member started to grow significantly (as shown in Figure 12a from the measurements of TR-8 and TR-9) and the consequent partial interaction decreased the flexural rigidity exhibited in the subsequent loading. A second reduction in flexural stiffness occurred near a load of 448 kN due to the slip starting to grow at the other member end (monitored with TR-6 and TR-7 as shown in Figure 12a). Specimen SF2 exhibited a similar response with an initial linear load-deflection branch (Figure 11b) whose slope was influenced by the development of slip at the two member ends (Figure 12b).

The deformations undergone by the two specimens were similar and, for this purpose, only those related to sample SF1 are presented. By considering the strain measurements of the steel section it was possible to observe that, while the steel remained below its elastic limit, the strain in the top part of the section highlighted that concrete had reached its crushing condition already at the end of the first load cycle, i.e. strain greater than 0.003 (noted by considering the readings of SG-1in Figure 13a, and SG-1bis1 in Figure 13b). By observing the strain distributions across the width of the slab at different levels of load, as depicted in Figure 14 by points P1, P2, P3 and P4, it can be noted that the cross-section did not remain plane due to shear-lag effects. This type of response was already reported for slim floor systems in [32] and widely studied in the literature for composite beams, e.g. [33-35].

Representative observations carried out at the end of the tests are reported in Figure 15. In particular, Figure 15a highlights the conditions of sample SF1 at the end of the experiment whose end slip is illustrated in Figure 15b. At the completion of the experiments, the samples were demolished to observe the deformations induced in the transverse reinforcing steel bars that were installed in the web holes.

Similar patterns were observed in both samples and, for this purpose, the deformed reinforcing bars of sample SF1 are presented in Figure 15c (only the middle part of the bar is shown). Figure 15d highlights the associated deformations that were noted on the edges of the web holes. As expected, the reinforcing bars closest to the beam ends were mostly deformed due to the partial interaction exhibited by the shear connection.

5. CONCLUSIONS

This paper presented new experimental data on the service and ultimate behaviour of slim floor beams. This form of construction is widely used for building applications. For the purpose of this study, two specimens were prepared and monitored over time for a period of about 10 months. The samples were identical in geometry and cast unpropped, and they differed only for the specified loading history. In particular, one sample was kept unloaded for the entire duration of the test while the second specimen was subjected to a sustained load after a period of about 3 months. Even if the long-term measurements started soon after the removal of the formwork, the time-dependent deformations associated with shrinkage were considered relatively small.

Despite the different loading history, both samples exhibited a similar ultimate response. This highlighted the fact that, for the adopted geometry and beam layout, creep effects did not influence the ultimate behaviour. Both samples failed in a ductile fashion by crushing of the concrete component. From strain measurements recorded across the width of the slab at mid-span it was possible to determine that shear-lag effects played an important role in the flexural response. The condition of the shear connection was evaluated at the end of the tests by removing the concrete. The steel reinforcing bars that had been initially installed through the web holes were deformed locally (at the web location) and these deformations increased significantly while moving towards the ends of the specimens. The shear connection deformability was also supported by the deformations of the edge holes. It is envisaged that

the experimental data reported in this study will be useful for the calibration and validation of numerical and design models related to the serviceability and ultimate limit states of slim floor systems.

6. ACKNOWLEDGEMENTS

The experimental work presented in this article was supported by the European Commission under its Research Programme of the Research Fund for Coal and Steel. The contribution of the third author was partly supported by the Australian Research Council through its Future Fellowship scheme (FT140100130). The Authors also gratefully acknowledge the work by the laboratory technicians of the University of Trento Stefano Girardi and Marco Graziadei.

7. REFERENCES

[1] Rackham JW, Couchman L and Hicks SJ (2009) Composite slabs and beams using steel decking: best practice for design and construction (Revised edition), The Metal Cladding & Roofing Manufacturers Association in partnership with The Steel Construction Institute.

[2] Lawson M, Beguin P, Obiala R and Braun M (2015) Slim-floor construction using hollow-core and composite decking systems, Steel Construction, 8(2), 85-89.

[3] Hicks S (2003) Current trends in modern floor construction. Magazine of the British Constructional Steelwork Association, 11(1), 32–33.

[4] Mullett DL (1992) Slim Floor Design and Construction, The Steel Construction Institute, Ascot, UK, Publication P110.

[5] Mullett DL (1998) Composite Floor Systems, Blackwell Science Ltd, Oxford, UK.

[6] Mullett DL and Lawson RM (1993) Slim Floor Construction Using Deep Decking, The Steel Construction Institute, Ascot, UK, Publication P127.

[7] Lawson RM, Mullett DL and Rackham JW (1997) Design of Asymmetric Slimflor Beams Using Deep Composite Decking, The Steel Construction Institute, Ascot, UK, Publication P175.

[8] Bernuzzi C, Gadotti F and Zandonini R (1995) Semi-continuity in slim floor steel-concrete composite systems, Proceedings of the 1995 1st European Conference on Steel Structures, EUROSTEEL'95, Athens, Greece, Balkema, Rotterdam, the Netherlands, 287–294.

[9] Bernuzzi C and Zandonini R (1995) Joint action in non-sway frames with steel-concrete composite slim floor beams, Journal of Singapore Structural Steel Society, 6(1), 75-85.

[10] Lawson RM, Bode H, Brekelmans JWPM, Wright PJ and Mullett DL (1999) 'Slimflor' and 'Slimdek' construction: European developments, Journal of Structural Engineering, 77(8), 22–30.

[11] Leskelä M (2002) Shallow Floor Integrated Beams and their Components: Comparison of Behavior, Proceedings of the Conference Composite Construction in Steel and Concrete IV, May 28 - June 2, 2000, Banff, Canada, American Society of Civil Engineers.

[12] Lawson RM, Lim J, Hicks SJ and Simms WI (2006) Design of composite asymmetric cellular beams and beams with large web openings, Journal of Constructional Steel Research, 62(6), 614–629.

[13] Braun M, Hechler O and Birarda V (2009) 140 m² Column Free Space due to Innovative Composite Slim floor Design, Proceedings of the 9th International Conference on Steel Concrete Composite and Hybrid Structures (ASCCS2009), Leeds (UK), 363 - 368.

[14] Wang Y, Yang L, Shi Y and Zhang R (2009) Loading capacity of composite slim frame beams, Journal of Constructional Steel Research, 65(3), 650–661.

[15] Hechler O, Braun M, Hauf G and Kuhlmann U (2011) CoSFB – The composite slim-floor beam, Eurosteel 2011 - 6th European Conference on Steel and Composite Structures, Budapest.

[16] Huo BY and D'Mello CA (2013) Shear transfer mechanisms in composite shallow cellular floor beams, Journal of Constructional Steel Research, 88(1), 191–205.

[17] Hechler O, Kuhlmann U, Eggert F, Hauf G, Braun M and Obiala R (2014) CoSFB - Composite Slim- Floor Beam - Experimental Test Campaign and Evaluation. Proceedings of the Conference

Composite Construction in Steel and Concrete VII, 28-31 July 2013, Palm Cove, Australia, American Society of Civil Engineers.

[18] Hauf G and Kuhlmann (2015) Deformation calculation methods for slim floors, Steel Construction, 8(2), 96-101.

[19] Lam D, Dai X, Kuhlmann U, Raichle J and Braun M (2015) Slim-floor construction – design for ultimate limit state, Steel Construction, 8(2), 79-84.

[20] Chen SM, Limazie T and Tan JY (2015) Flexural behavior of shallow cellular composite floor beams with innovative shear connections, Journal of Constructional Steel Research, 106(1), 329–346.

[21] Limazie T and Chen SM (2016) FE modeling and numerical investigation of shallow cellular composite floor beams, Journal of Constructional Steel Research, 119(1), 190–201.

[22] Limazie T and Chen SM (2017) Effective shear connection for shallow cellular composite floor beams. Journal of Constructional Steel Research, 128(1), 772–788.

[23] Chen S and Limazie T (2017) Composite slim floor beams with innovative shear connections, Proceedings of the Institution of Civil Engineers: Structures and Buildings, 171(SB1), 29-37.

[24] Ranzi G, Leoni G and Zandonini R (2013) State of the art on the time-dependent behaviour of composite steel-concrete structures, Journal of Constructional Steel Research, 80, 252-263.

[25] EN 1994-1-1 (2004) EUROCODE 4: Design of composite steel and concrete structures - Part 1-1: General rules and rules for buildings, European Committee for Standardization.

[26] Hauf G, Kuhlmann U (2015) Deformation calculation methods for slim floors, Steel Construction, 8(2), 96-101.

[27] Al-Deen S, Ranzi G and Vrcelj Z (2011) Full-scale long-term experiments on simply-supported composite beams with solid slabs, Journal of Constructional Steel Research, 67(3), 308-321.

[28] Al-Deen S, Ranzi G, and Vrcelj Z (2011) Full-scale long-term and ultimate experiments of simply-supported composite beams with steel deck, Journal of Constructional Steel Research, 67(10), 1658-1676.

[29] Ranzi G, Al-Deen S, Ambrogi L and Uy B (2013) Long-term behaviour of simply-supported post-tensioned composite slabs, Journal of Constructional Steel Research, 88, 172-180.

[30] Ranzi G (2018) Service design approach for composite steel-concrete floors, Proceedings of the Institution of Civil Engineers - Structures and Buildings, 171(1), 38-49.

[31] Braun M, Obiala R, Odenbreit C (2015) Analyses of the loadbearing behaviour of deep-embedded concrete dowels, CoSFB, Steel Construction, 8(3), 167-173.

[32] Hauf G and Kuhlman U (2015) Deformation calculation methods for slim floors, Steel Construction, 8(2), 96-101.

[33] Dezi L, Gara F, Leoni G and Tarantino A (2001) Time-dependent analysis of shear-lag effect in composite beams, Journal of Engineering Mechanics ASCE, 127(1), 71-79.

[34] Macorini L, Fragiacomo M, Amadio C and Izzuddin BA (2006) Long-term analysis of steel-concrete composite beams: FE modelling for effective width evaluation, Engineering Structures, 28, 1110-1121.

[35] Gara F, Leoni G and Dezi L (2009) A beam finite element including shear lag effect for time-dependent analysis of steel-concrete composite decks, Engineering Structures, 31, 1888-1902.

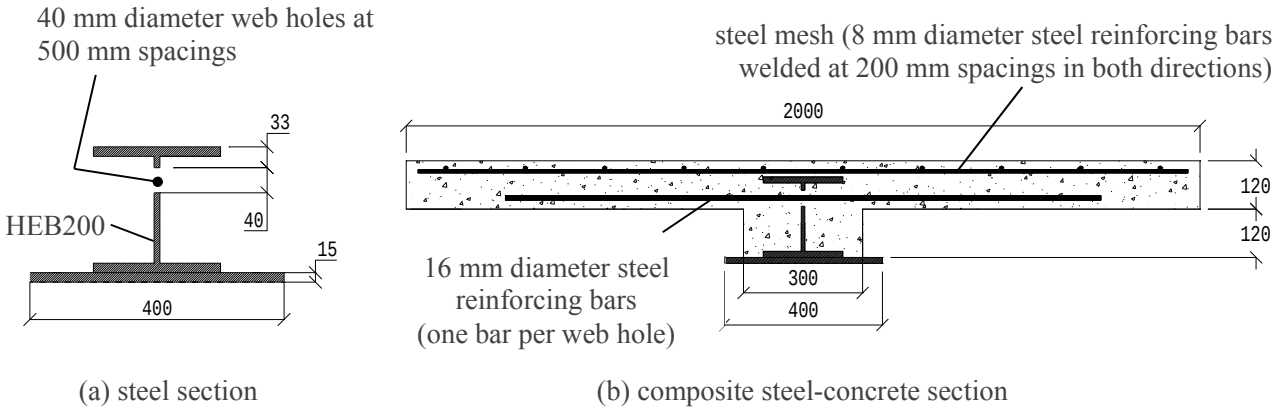

(a) steel section

(b) composite steel-concrete section

Note: all dimensions in mm

Figure 1: Cross-sectional geometry of the slim floor samples

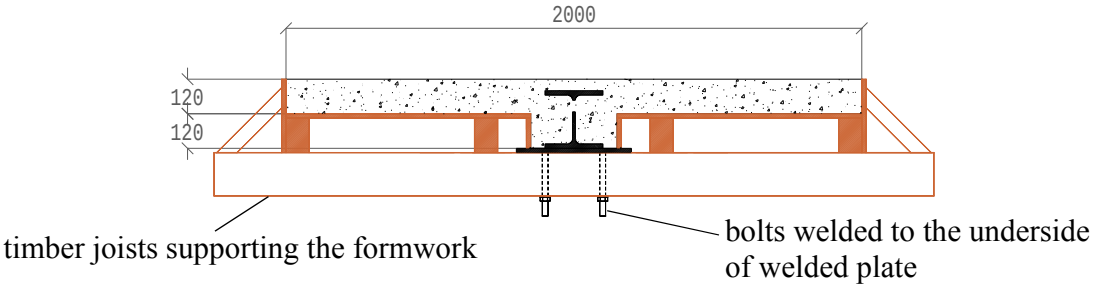

(a) cross-sectional view of the formwork arrangement

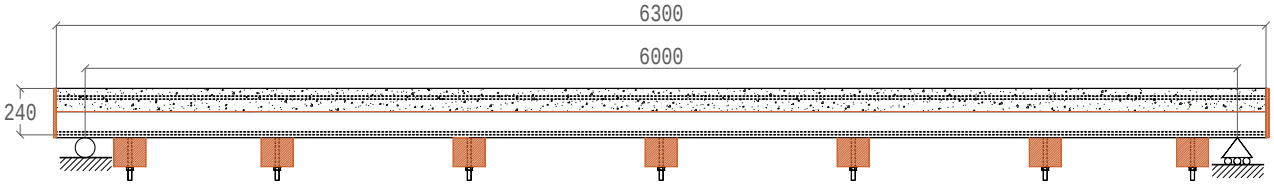

(b) elevation showing the formwork arrangement

(c) overview of the sample preparation

Note: all dimensions in mm

Figure 2: Layout of the formwork arrangement and sample preparation for unpropped construction

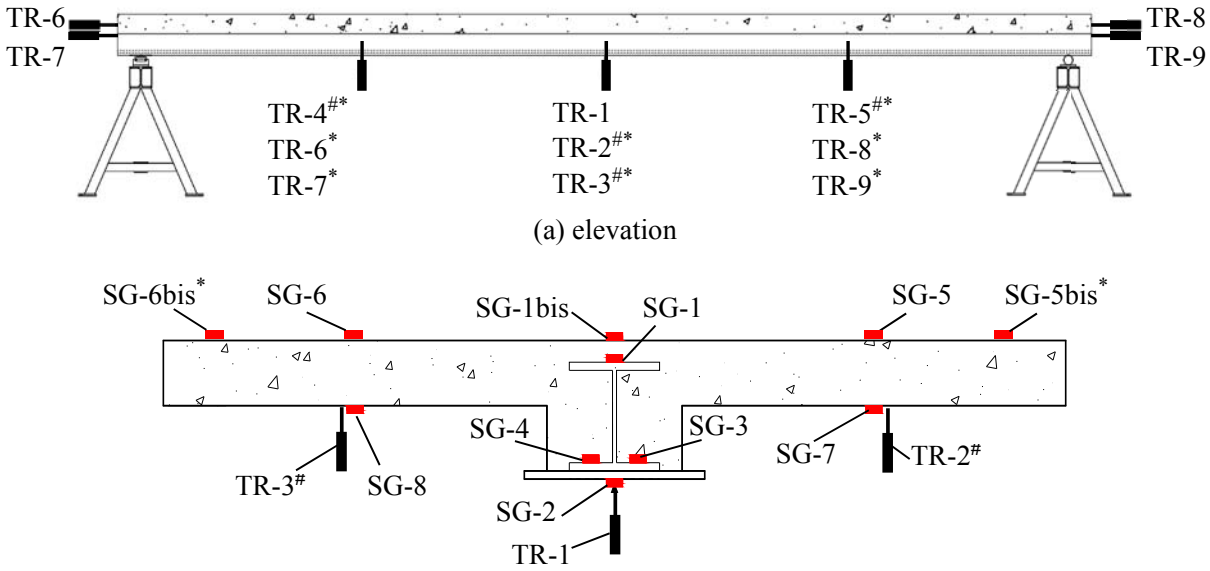

Figure 3: Instrumentation layout

(a)

(b)

(c)

(d)

Figure 4: Application of the sustained load on sample SF2

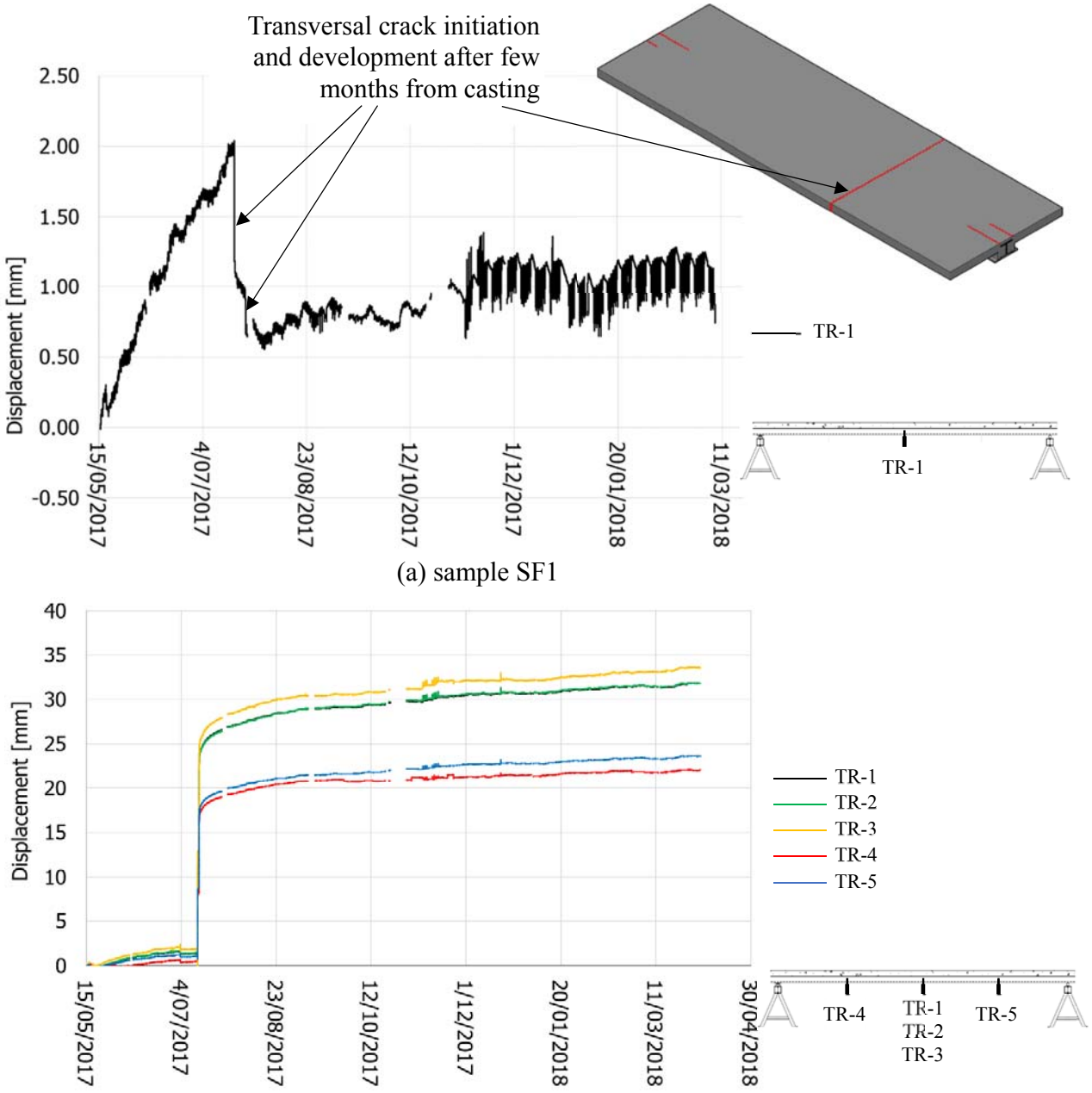

Note: positive displacements represent downward deflections.

Figure 5: Long-term experiment: deflection measurements

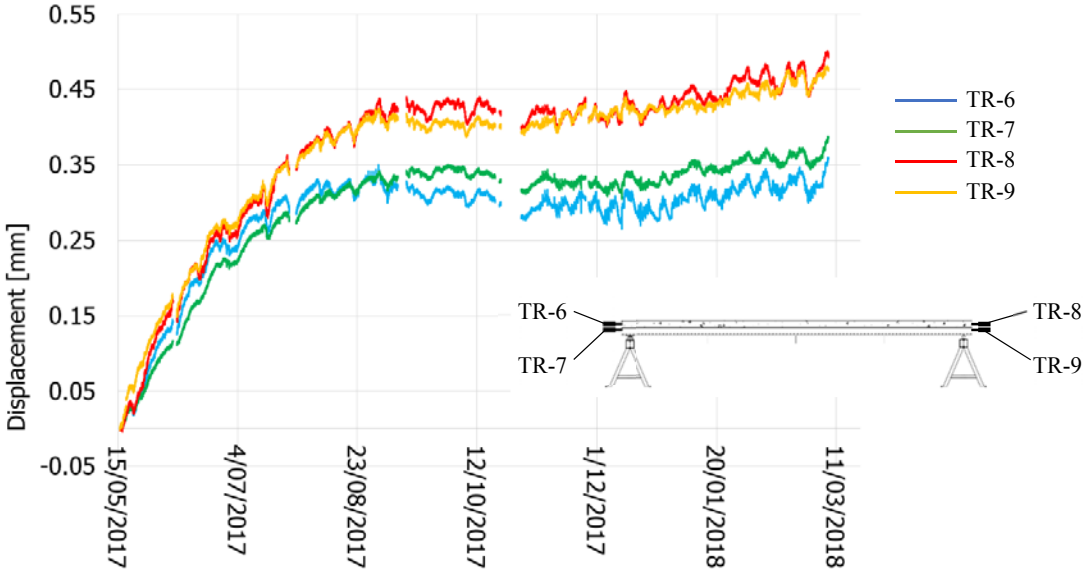

(a) sample SF1

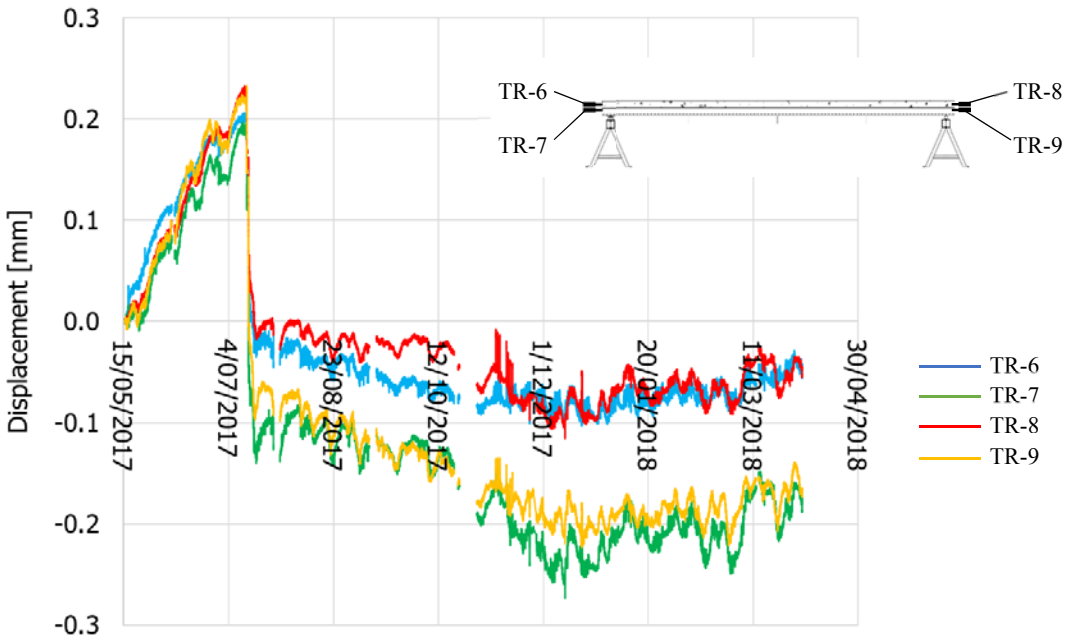

(b) sample SF2

Note: positive displacements represent the situation in which the concrete component moves inwards (towards the mid-span) relative to the steel component, therefore exposing the end of the steel component.

Figure 6: Long-term experiment: end slip measurements

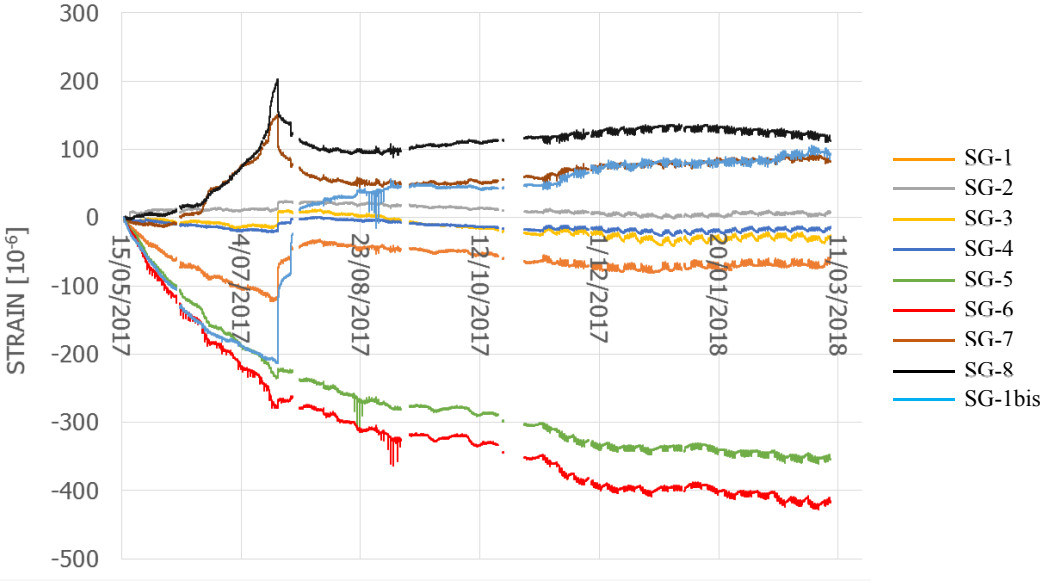

(a) sample SF1

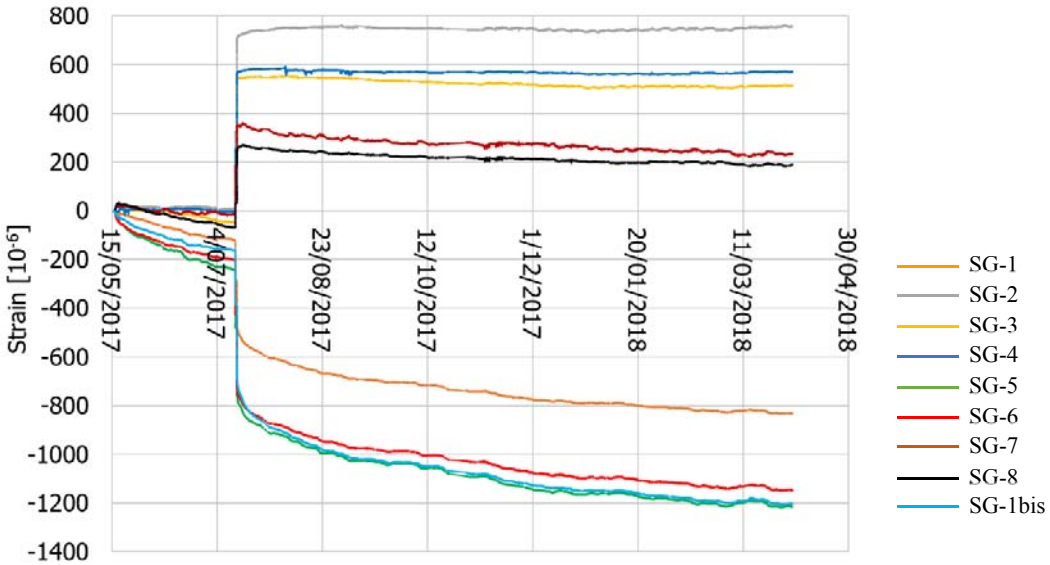

(b) sample SF2

Figure 7: Long-term experiment: strain measurements

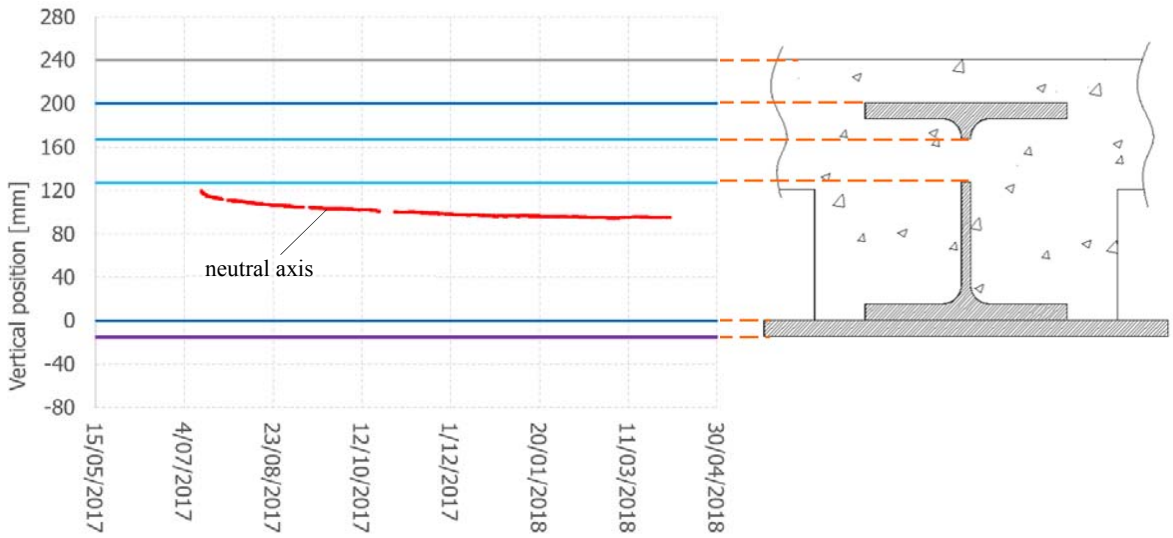

Figure 8: Time-dependent variation of the neutral axis for sample SF2 after the application of the sustained load

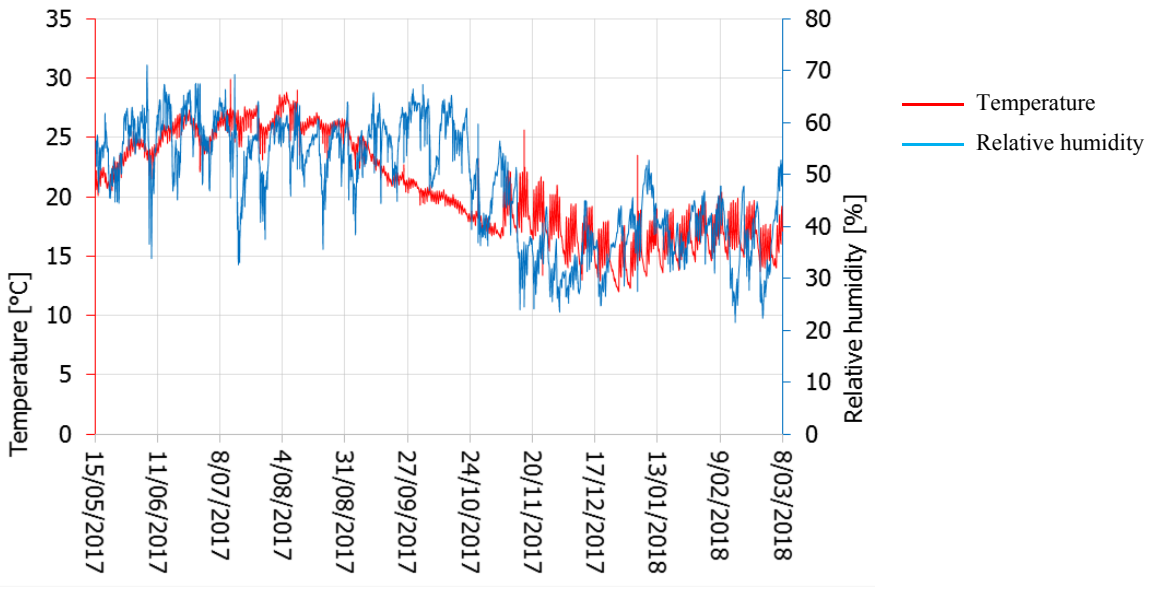

Figure 9: Variations of temperature and relative humidity during long-term tests

Figure 10: Test setup

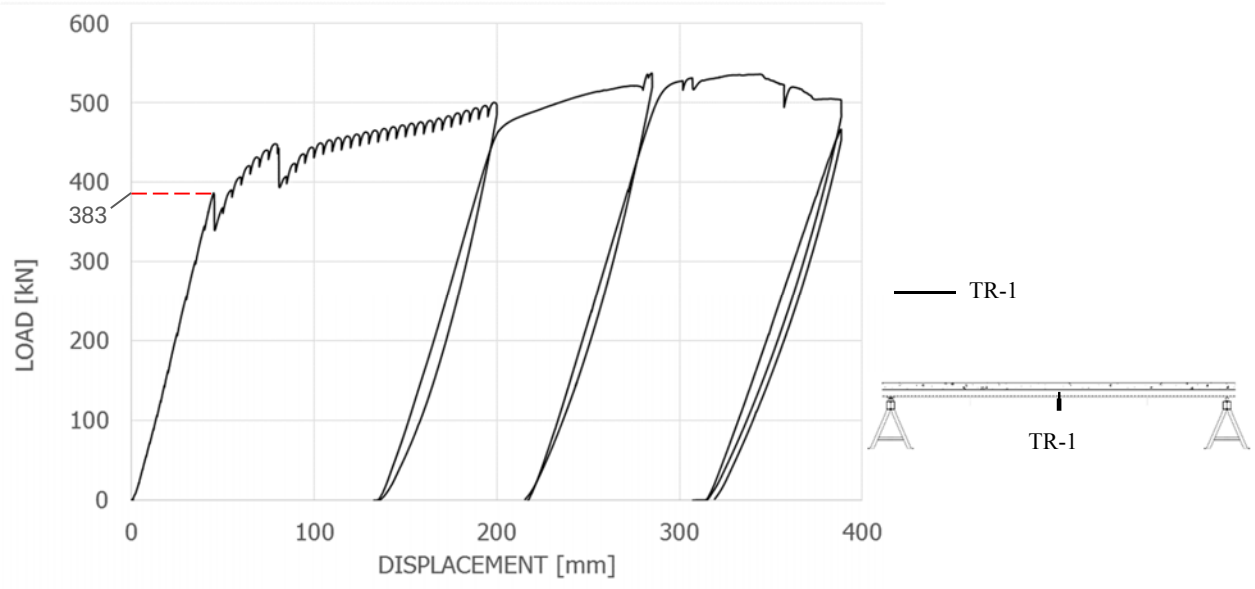

(a) sample SF1

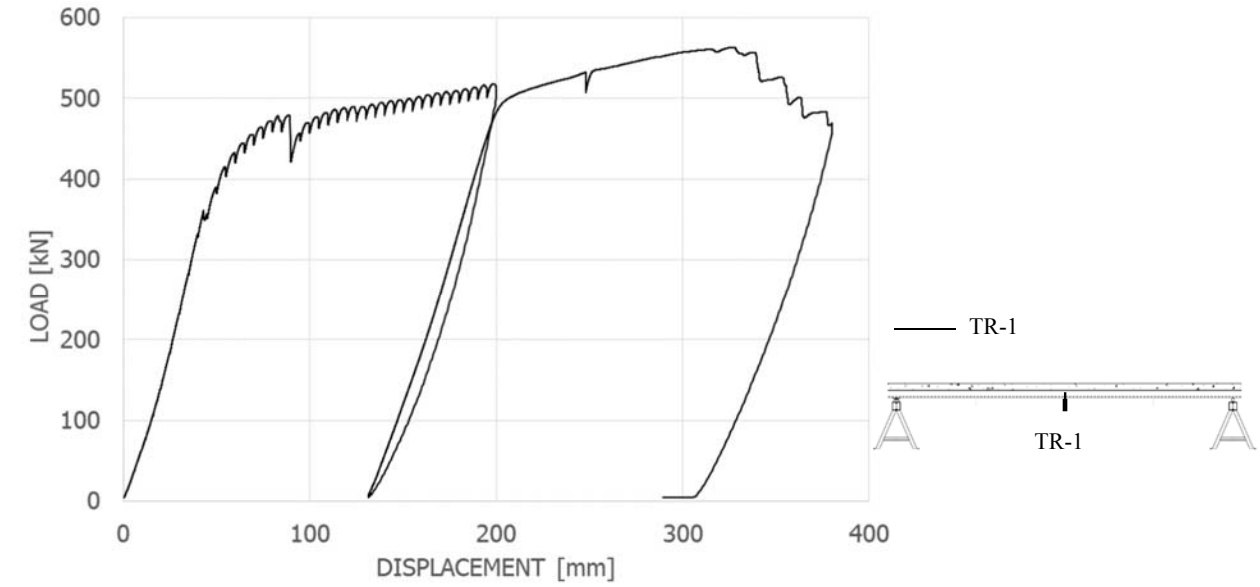

(b) sample SF2

Figure 11: Ultimate experiment: deflection measurements

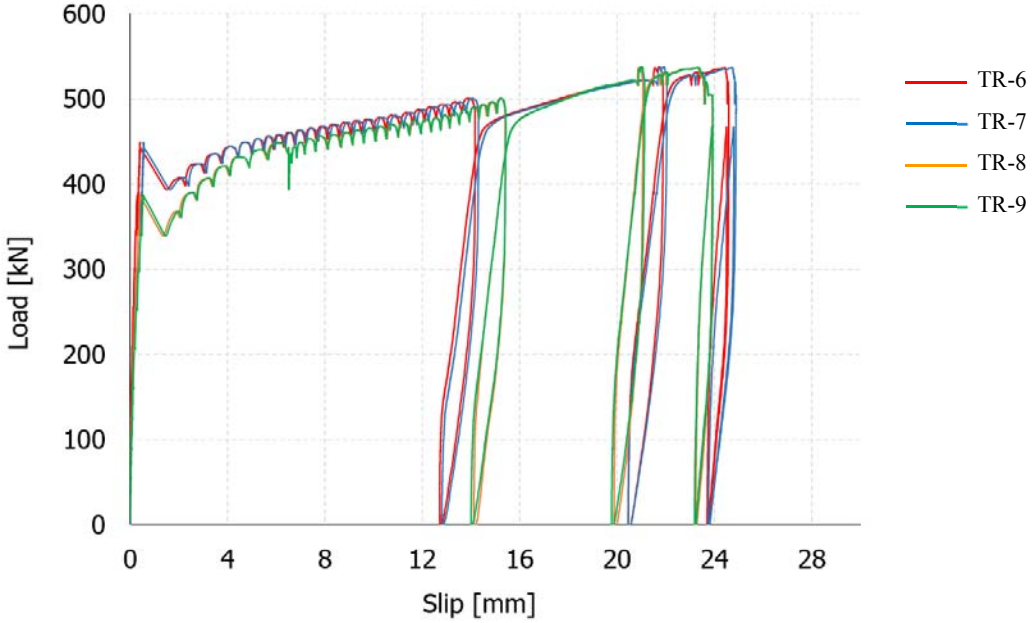

(a) sample SF1

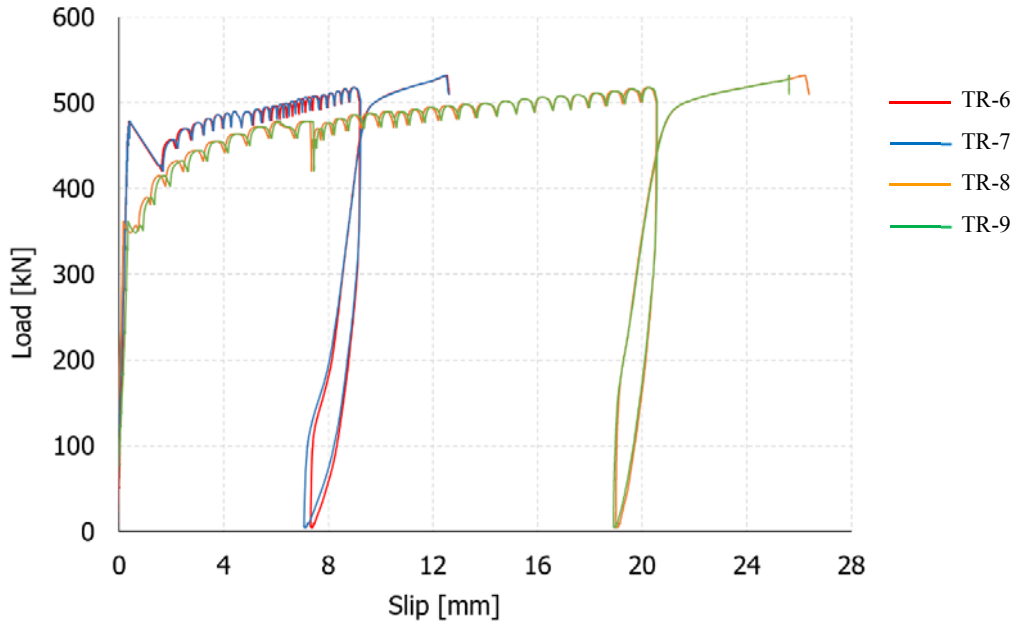

(b) sample SF2

Note: positive displacements represent the situation in which the concrete component moves away from the mid-span relative to the steel component, therefore hiding the end of the steel component as shown in Figure 15b.

Figure 12: Ultimate experiment: slip measurements

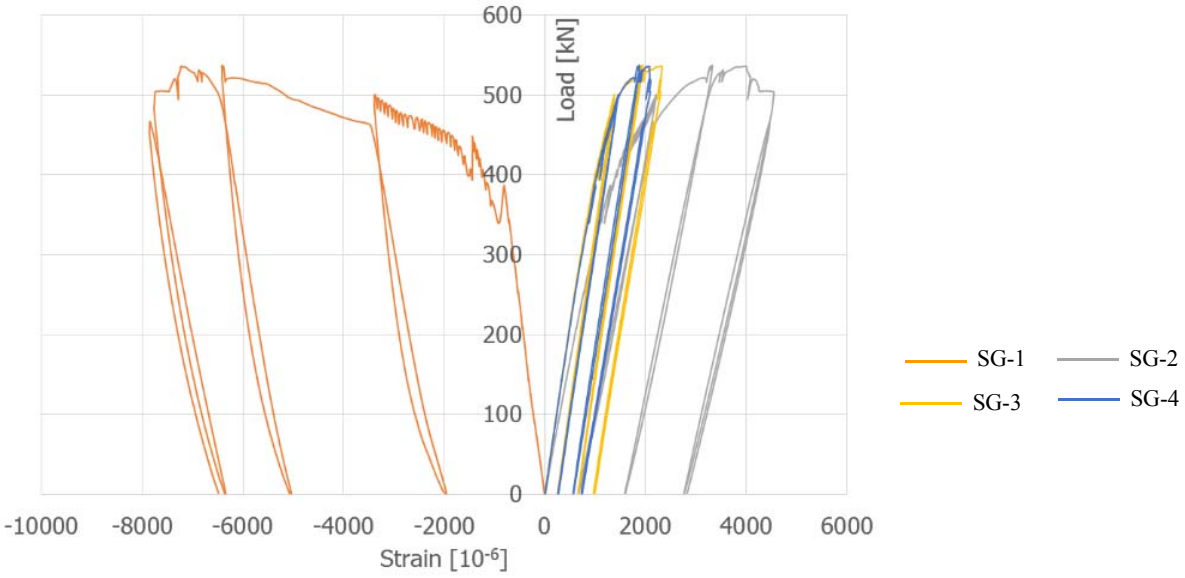

(a) strain readings in the steel

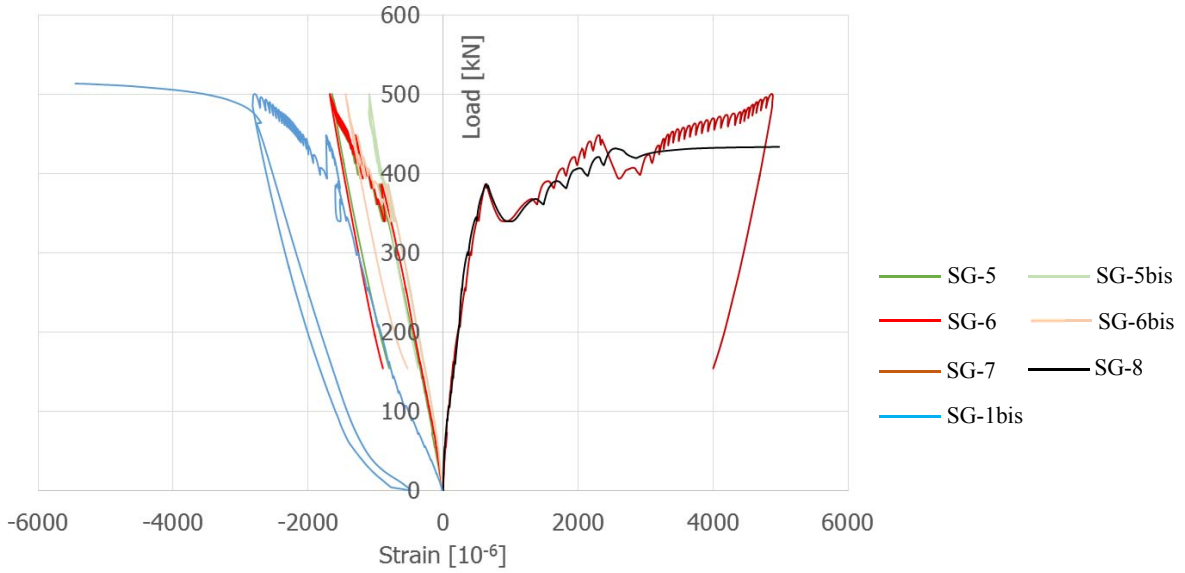

(b) strain readings in the concrete

Figure 13: Ultimate experiment: strain measurements of sample SF1

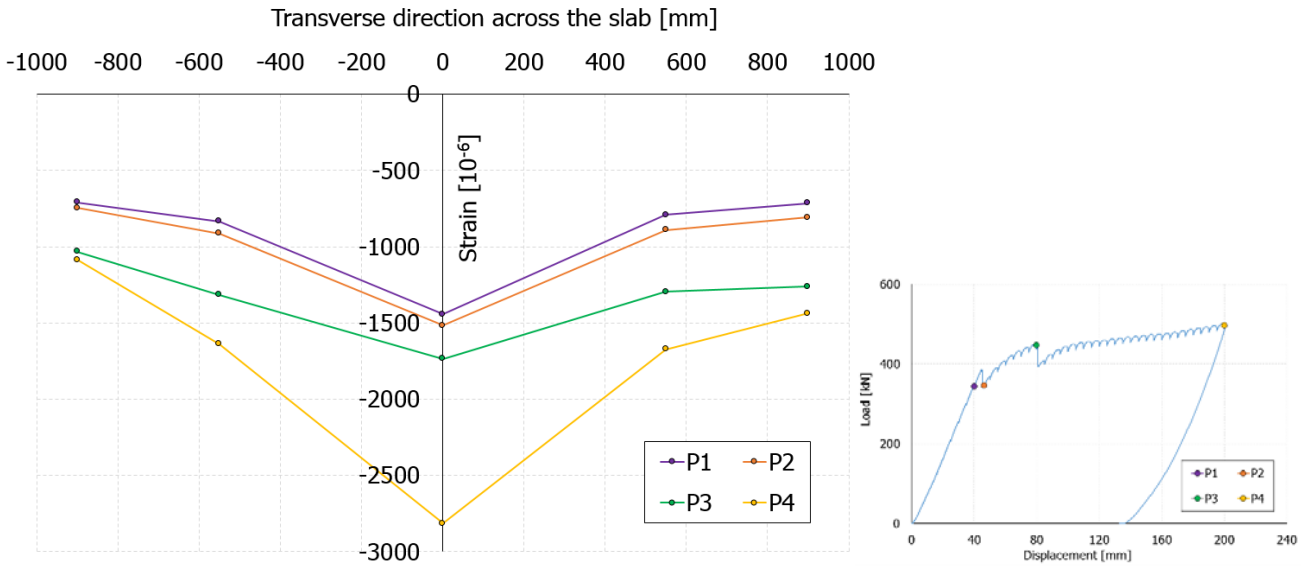

Figure 14: Ultimate experiment: shear-lag behaviour at mid-span of sample SF1 for first load cycle

(a) overview of sample

(b) end slip

(c) steel reinforcing bars

(d) deformations in the holes of the steel web after completion of the tests

Figure 15 Representative observations at the completion of the ultimate tests (sample SF1)